Atomtronic multiterminal Aharonov-Bohm interferometer

Jonathan Wei Zhong Lau,[1,*] Koon Siang Gan,[1] Rainer Dumke,[1,2] Luigi Amico,[1,3,4,5,†]
Leong-Chuan Kwek,[1,6,7,8] and Tobias Haug [9,‡]

[1]*Centre for Quantum Technologies, National University of Singapore, Singapore 117543, Singapore*
[2]*School of Physical and Mathematical Sciences, Nanyang Technological University, Singapore 637371, Singapore*
[3]*Quantum Research Center, Technology Innovation Institute, Abu Dhabi 9639, UAE*
[4]*INFN-Sezione di Catania, Via S. Sofia 64, 95127 Catania, Italy*
[5]*LANEF 'Chaire d'excellence,' Universitè Grenoble-Alpes & CNRS, F-38000 Grenoble, France*
[6]*MajuLab, CNRS-UNS-NUS-NTU International Joint Research Unit, Singapore UMI 3654, Singapore*
[7]*National Institute of Education, Nanyang Technological University, 1 Nanyang Walk, Singapore 637616, Singapore*
[8]*School of Electrical and Electronic Engineering Block S2.1, 50 Nanyang Avenue, Singapore 639798, Singapore*
[9]*QOLS, Blackett Laboratory, Imperial College London, London SW7 2AZ, United Kingdom, Singapore*

We study a multifunctional device for cold atoms consisting of a three-terminal ring circuit pierced by a synthetic magnetic flux, where the ring can be continuous or discretized. The flux controls the atomic current through the ring via the Aharonov-Bohm effect. Our device shows a flux-induced transition of reflections from an Andreev-like negative density to positive density. Further, the flux can direct the atomic current into specific output ports, realizing a flexible nonreciprocal switch to connect multiple atomic systems or sense rotations. By changing the flux linearly in time, we convert constant matter wave currents into an ac modulated current. This effect can be used to realize an atomic frequency generator and study fundamental problems related to the Aharonov-Bohm effect. We experimentally demonstrate Bose-Einstein condensation into the light-shaped optical potential of the three-terminal ring. Our work opens up the possibility of atomtronic devices for practical applications in quantum technologies.

Precise control over quantum systems has led to the rapid development of quantum technologies for applications in quantum simulation [1], quantum communication [2], and metrology [3]. These latter fields are fundamental to atomtronics [4], an emerging quantum technology of propagating cold atoms in matter-wave circuits [3–5]. Inspired originally by electronics, atomtronics exploits the advancement in optical traps and cooling to precisely move ultracold atoms to realize novel and practical quantum devices [6–9]. Indeed, simple atomtronic circuits with Bose-Einstein condensates (BECs) or degenerate fermions that mimic classical transport have already exhibited interesting physics with potential applications [10–22].

The construction of atomtronic circuits requires an indepth understanding of cold-atom transport both theoretically and experimentally [1,16,23–28]. Analogs of one-dimensional mesoscopic conductors also have been investigated [29–33], with transport now possible over macroscopic distances [34]. In particular, BECs trapped in ring shaped potentials [35–38] and Y-shaped junctions [7,39,40] augurs potential practical applications due to its subtle similarity to integrated photonic chips.

A promising geometry for cold atom devices is the ring-shaped circuit. Such systems can exhibit superfluid current flows [20,41–43] and can realize effective two-level dynamics for a potential atomtronic qubit [44,45]. Here, the transport can be controlled by the Aharonov-Bohm effect where the magnetic flux through the ring changes the interference of matter [46]. The static Aharonov-Bohm effect controls the conductance in mesoscopic electronic rings [47–50], while the nature of the time-dependent Aharonov-Bohm effect is still controversially discussed [51–54]. Through the application of suitable synthetic fields [19,20,55–59], cold atoms can harness the Aharonov-Bohm effect with a high degree of control and coherence that is difficult to reach in other systems. An important example is the transport through two-terminal Aharonov-Bohm rings with bosonic atoms [37,39,40].

Here, we study the transport in a three terminal circuit in which a bosonic condensate is guided from a source lead through a Aharonov-Bohm ring attached to two drains— see Fig. 1(a). We simulate this system with extensive leads coupled to a continuous 2D ring or a discretized ring of three sites. We show an experimental demonstration of the

---
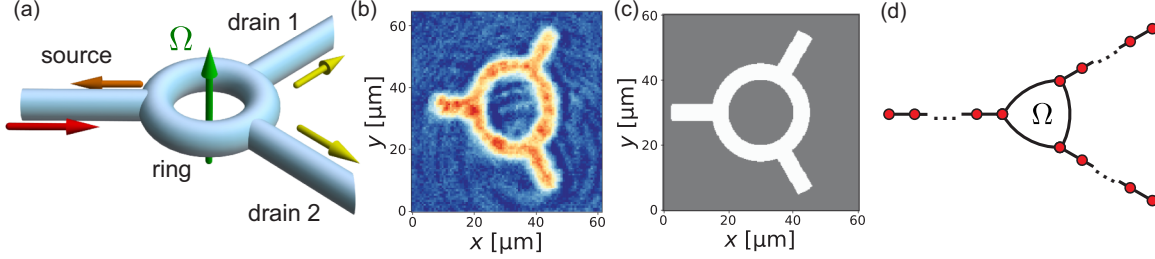
FIG. 1. (a) Three-terminal Aharonov-Bohm circuit with source lead (left) attached to a ring with two drain leads (right). A synthetic Aharonov-Bohm flux Ω through the ring controls the current flowing from source to the drains, which can be used for multiple functionalities. (b) An initial experimental demonstration of the setup with a BEC. 6×10^4 rubidium atoms are cooled to 50 nK by atom evaporation into an optical potential created by a DMD. We show the *in situ* atomic density measured with absorption imaging. (c) Potential of a two-dimensional ring-lead system simulated with GPE with ring diameter $R = 30$ μm. (d) Sketch of lattice ring-lead system for Bose-Hubbard simulations. Source and drain leads consist of an extensive number of lattice sites, connected to an $L = 3$ site ring.

continuous setup by loading a Bose-Einstein condensate (BEC) of ^{87}Rb atoms in a digital micromirror device (DMD) generated optical potential—see Fig. 1(b). We demonstrate that our scheme provides a useful concept for a multifunctional device. The applications of our work are summarized in Fig. 2. We show that our system can (i) control density waves, (ii) realize a nonreciprocal switch and sense rotations, and (iii) convert a direct current (dc) matter-wave into an alternating current (ac) modulation of the dc matter wave.

We first introduce the system together with an experimental demonstration of the setup. We then analyze the low energy and highly nonequilibrium dynamics of the system as well as the dynamics under a time-dependent driving of the flux. We finally discuss the applications of our work.

Model. A sketch of the three-terminal ring pierced by flux Ω is shown in Fig. 1(a). We experimentally demonstrate the feasibility of this setup by loading a BEC into a static optical potential generated by a digital micromirror device [see Fig. 1(b) and the Supplemental Material (SM) F [60] for details]. In the dilute limit with weak interactions, we simulate the setup with the 2D Gross-Pitaevskii equation (GPE)

$$i\hbar\partial_t\psi = \left[-\frac{\hbar}{2m}(\partial_x^2 + \partial_y^2) + V(x,y) + g_{2D}N|\psi|^2 + \omega L_z\right]\psi,$$

where $\psi \equiv \psi(x,y,t)$ is the wave function, m is the mass of the atoms, g_{2D} is the atom-atom interaction strength for rubidium atoms in two dimensions [61], ω is the rotation of
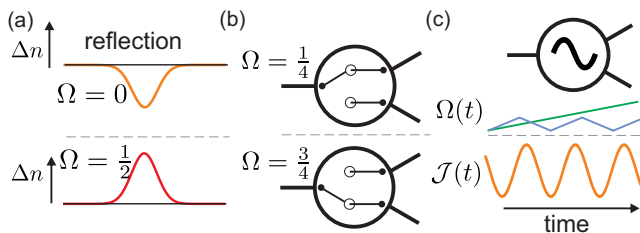
FIG. 2. Applications of three-terminal cold atom Aharonov-Bohm circuit. (a) Control reflections of density waves from negative (Andreev-like) to positive with flux Ω. (b) Directional switch of the current to one of the output terminals by adjusting Ω, which can also be used as a rotation sensor. (c) Atomic frequency generator with a sinusoidal output current $\mathcal{J}(t)$ of period T by linearly increasing $\Omega(t) = t/T$ in time or via a periodic ramp.

the system to induce flux, $L_z = -i(x\partial_y - y\partial_x)$ is the angular momentum operator, and N is the number of atoms. The potential $V(x,y)$ is shown in Fig. 1(c).

In the limit where leads and ring are strongly confined, we can treat the system as effectively one dimensional. Here, we simulate this system numerically for different interaction strengths with the Bose-Hubbard model by dividing the system into the source lead, two drain leads, and the ring with L sites [see Fig. 1(d)]. The source lead s and the two drains b, c are connected to the ring in a symmetric manner with $x_s = 1$, $x_b = L/3$, and $x_c = 2L/3$. We choose an extensive number of source and drain sites, while the ring is assumed to be small with $L = 3$ sites. The system Hamiltonian $H = H_r + H_\ell + H_{r\ell}$ with N bosons is given by

$$H_r = \sum_{j=1}^{L}\left[\frac{U}{2}\hat{n}_j(\hat{n}_j - 1) - J(e^{-i2\pi\Omega(t)/L}\hat{a}_{j+1}^\dagger\hat{a}_j + \text{H.c.})\right],$$

$$H_{r\ell} = -K\sum_{\alpha=\{b,c,s\}}(\hat{a}_1^\dagger\hat{a}_{x_\alpha} + \text{H.c.}),$$

$$H_\ell = \sum_{\alpha=\{b,c,s\}}\sum_{j=1}^{L_\alpha}\left[\frac{U_\alpha}{2}\hat{n}_j^\alpha(\hat{n}_j^\alpha - 1) - J_\alpha(\hat{\alpha}_{j+1}^\dagger\hat{\alpha}_j + \text{H.c.})\right],$$

$$(1)$$

where $\hat{a}_j(\hat{a}_j^\dagger)$ is the bosonic annihilation (creation) operator at site j on the ring, $\hat{n}_j = \hat{a}_j^\dagger\hat{a}_j$ is the corresponding number operator, J is the intraring coupling strength, and U is the interaction strength of the ring. We impose periodic boundary conditions in the ring $\hat{a}_{L+1} = \hat{a}_1$. For the leads, $\hat{\alpha}_j$ is the annihilation operator, $\hat{n}_j^\alpha$ the number operator, L_α the number of sites, U_α the interaction strength, and J_α the intrareservoir couplings for the source and drains with $\alpha \in \{s, b, c\}$.

$\Omega(t)$ represents the flux through the ring which can be dependent on time t. This flux can be generated for neutral atoms via rotation, where the Coriolis flux mimics the effect of the magnetic field [20,62]. A suitable approach is to rotate the whole potential with rotational frequency $\omega = \frac{\Omega\hbar}{mR^2}$, where R is the radius of the ring, yielding $\omega = 5.1\Omega$ Hz for the parameters of Fig. 1(b) [20,35]. The undesired centrifugal potential can be removed with the correction potential $V(r) = \frac{1}{2}\omega^2r^2$, where r is the distance to the rotation center. As an alternative approach, synthetic magnetic fields can be achieved
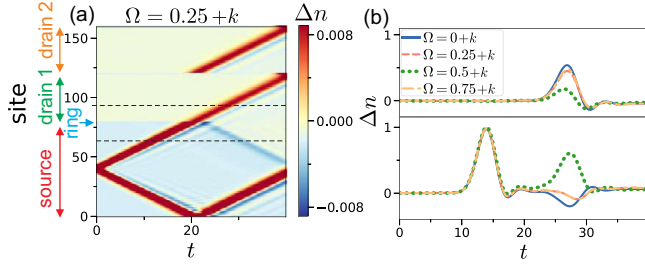
FIG. 3. Dynamics of low-energy excitations in a three-terminal ring device for $L = 3$ ring sites. (a) Change of density relative to average density $\Delta n(t) = \langle n(t) \rangle - n_0$ as a function of time and sites of source, ring, and drain 1 and 2 for $\Omega = \frac{1}{4} + k$, where k is an integer. The forward propagating wave is transmitted into the drains, as well as reflected back into the source. (b) Δn in source (bottom) and first drain (top) measured at positions shown as dashed lines in (a). We show $N = 80$ hard-core bosons with $J = 1$, $K = 0.5$ and in total $L = 160$ lattice sites ($L = 3$, $L_s = 79$, and $L_b = L_c = 39$).

by counterpropagating Raman beams [56,57] or driving the optical potential in time [63], which has been demonstrated for lattice systems [64]. Due to flux quantization in the ring, the spectrum of $H(\Omega)$ is periodic with $\Omega \rightarrow \Omega + k$, k being integer, with the flux quantum set to 1. The current operator between lead α and ring is given by $\mathcal{J}_\alpha = -iK(\hat{a}_1^\dagger \hat{a}_{x_\alpha} - \text{H.c.})$.

Low-energy dynamics. First, we study the dynamics close to the ground state using the Bose-Hubbard model. We perturb the local potential in the source $H_e = -\epsilon_s \sum_{j=1}^{L_s} \exp[-(j - D)^2/2\sigma^2]\hat{n}_j^s$, with $D = L_s/2$, $\sigma = 2$, and $\epsilon_s = 0.3$, We prepare the ground state of the Hamiltonian $H + H_e$, where now H_e leads to a locally raised density in the source. At $t > 0$, we evolve the system with H only, resulting in two density waves traveling in positive and negative direction (the negative direction can be ignored for a sufficiently large source). We investigate the change in density $\Delta n(t) = \langle n(t) \rangle - n_0$, where n_0 is the average density. The dynamics is calculated using matrix product states with the ITensor library [65]. In Fig. 3(a) we show $\Delta n(t)$ for $\Omega = \frac{1}{4} + k$ as a function of time t and the sites of source, ring, and drain (see SM B [60] for other values of Ω). The forward propagating density wave moves from the source to the ring, then is transmitted into the drains as well as reflected back to the source. For any value of Ω the transmission into drain 1 and drain 2 is nearly the same. We show the density Δn at a fixed site in source and drain in Fig. 3(b). The transmission is maximal for $\Omega = k$ and minimal for $\Omega = \frac{1}{2} + k$. We observe identical results for $\Omega = \frac{1}{4} + k$ and $\Omega = \frac{3}{4} + k$, which is the result of an emergent reflection symmetry $\Omega \rightarrow -\Omega$. We find that the reflection into the source at a specific time t_r [$t_r \sim 27$ in Fig. 3(b)] changes in nature with Ω. For $\Omega = k$ we find a clear negative reflection, which is a hallmark of Andreev reflections. With increasing Ω, the Andreev reflections turn into positive reflections.

Dynamics far from ground state. We investigate the dynamics when the system is far from the ground state via a quench protocol. At $t > 0$, the filled source lead injects atoms into the initially empty ring and drains. We study this highly nonequilibrium setting for zero, weak, and infinite interaction.

In the limit of zero interaction $U = 0$, we describe the dynamics with the Landauer formalism as explained in SM

A [60], which yields a transmission of

$$G_\alpha = 16\left|\frac{1 - \sqrt{2} + 2i(2\sqrt{2} - 3)\exp[-i\pi(2\Omega + \alpha)]}{62 - 46\sqrt{2} + 2i\cos[\pi(2\Omega + \alpha)]}\right|^2 \quad (2)$$

into the respective drains $\alpha \in \{1, 2\}$. The resulting transmission and reflection of the system is shown in Fig. 4(a). For $\Omega = \frac{1}{4}$ we have unit transmission into drain 1 and zero transmission into drain 2, while for $\Omega = \frac{3}{4}$ the dynamics of the drains is interchanged. Thus tuning Ω can direct the current either into drain 1 or drain 2, realizing a perfect nonreciprocal switch with zero backreflection.

Next, we investigate the system in the dilute limit with the continuous 2D GPE [66]. In Fig. 4(b), we find that physically rotating the setup with Ω modulates the average fraction of atoms in the drains. The flux dependence of the current arises from interference patterns in the ring, which are modulated by Ω. Increasing interaction leads to smaller interference patterns, which reduces the flux sensitivity. Due to the finite width of the ring and the radial dependence of the flux, we find that the system is not perfectly periodic with Ω in contrast to the one-dimensional case. By reducing the width of the ring and leads we expect that the symmetry can be restored. Further details are shown in SM G [60].

Now, we investigate the limit of strong interaction with hard-core bosons, where each lattice site occupies at most one boson. We use $L = 3$ ring sites and simplify the source and drain leads by tracing out all of their sites except the very first one coupled to the ring ($\hat{s}_1$, $\hat{b}_1$, and $\hat{c}_1$). The dynamics of the reduced density matrix $\rho(t)$ within the Born-Markov approximation is described by [39,67]

$$\frac{\partial \rho}{\partial t} = -\frac{i}{\hbar}[H, \rho] - \frac{1}{2}\sum_m\{L_m^\dagger L_m, \rho\} + \sum_m L_m \rho L_m^\dagger, \quad (3)$$

with the Lindblad operators $L_1 = B_s\hat{s}_1^\dagger$, $L_2 = B_b\hat{b}_1$, $L_3 = B_c\hat{c}_1$, and coupling strength B_α. L_1 describes bosons entering the system at the source site and L_2, L_3 atoms leaving to the respective drains. We solve for the steady-state ρ_{ss} via $\partial \rho_{ss}/\partial t = 0$ [68]. In Fig. 4(c) we show the steady-state current $\mathcal{J}(\Omega)$. The current in drain 1 and 2 varies strongly with Ω, allowing for directional control into either drain. The source current shows a transition from being flux independent to flux dependent with intraring coupling J (see SM C [60]).

Time-dependent flux. The flux $\Omega(t) = t/T$ is now linearly increased in time by one flux quantum for one period T. As a result, the current undergoes a periodic modulation. For $t > 0$, we inject atoms via the source into the initially empty ring and drains for the lattice Bose-Hubbard model. We show the case of $T = 2.8$ in Fig. 5(a). The current undergoes initial transient dynamics until it settles into periodic sinusoidal oscillations, where the currents in the two drains are shifted by $T/2$. The drain current oscillates between close to 0 and nearly the magnitude of the source current. Thus this device realizes a form of atomic dc/ac converter where a constant source current converts into ac modulated currents.

We investigate the conversion efficiency $C = \Delta\mathcal{J}_{\text{drain}}/\max(\mathcal{J}_{\text{source}})$ of the dc/ac converter as a function of T and J in Fig. 5(b). $C = 1$ indicates that the amplitude of the drain current oscillation matches the
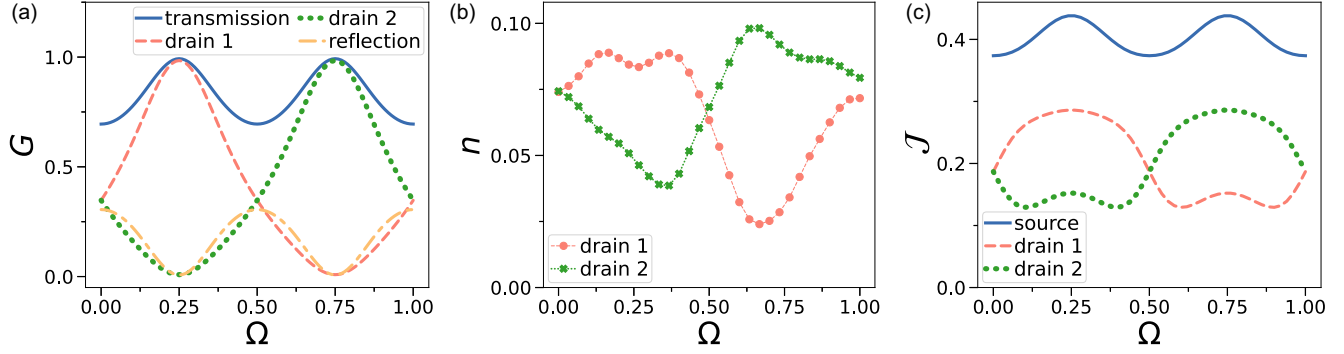
FIG. 4. Transport through a three-terminal device for the nonequilibrium setting and different interaction strengths. (a) Landauer formalism for noninteracting bosons. We show the total transmission and reflection of the system, as well as the transmission into drain 1 and 2 as a function of flux Ω. (b) Atom fraction n in the drain averaged over time $t = 400$ ms for a continuous ring-lead system with the 2D GPE. $N = 2000$ atoms are initially prepared in the source and evolved in the potential shown in Fig. 1(c), where the physical rotation frequency is given by $\omega = \frac{\Omega \hbar}{mR^2}$. (c) Steady-state current $\mathcal{J}$ for hard-core bosons and $L = 3$ ring sites as a function of flux Ω for $J = 1$, $L = 3$, $K = 1$, and $B_s = B_d = 1$.

source current. We define the drain current amplitude $\Delta \mathcal{J}_{\text{drain}} = \max_{t/T \gg 1} \mathcal{J}_{\text{drain}}(t) - \min_{t/T \gg 1} \mathcal{J}_{\text{drain}}(t)$ and the maximal source current $\max(\mathcal{J}_{\text{source}}) = \max_{t/T \gg 1} \mathcal{J}_{\text{source}}(t)$, where we take the maximum over the long-time behavior $t/T \gg 1$. For small T, the driving is much faster than the system dynamics which suppresses large oscillations. For large T, the driving is much slower than the system dynamics, causing it to be dominated by the properties of the instantaneous steady state as a function of Ω (see SM D [60]). We find a sweet spot in the regime of intermediate $T \approx 2.8$ with $C \approx 0.88$ for $J = \frac{1}{2}$. While increasing the flux linearly might be experimentally difficult, similar results can achieved by a simple periodic modulation between $\Omega = 0$ and $\Omega = 1$ as shown in SM E [60].

Discussion. We propose a multifunctional atomtronic device with a three-terminal ring circuit. We study the setup with a continuous potential as well as a lattice with $L = 3$ ring sites and extensive leads. In the low-energy regime for the lattice setup, transport through the device is realized with density waves. The flux controls the conductance of the source-ring interface yielding a maximal current for $\Omega = 0$ and minimal for $\Omega = \frac{1}{2}$. By tuning Ω, our setup controls the type of reflection with a crossover from negative Andreev-like to a normal

one. This effect opens up another way to control the transport of density waves, as well as detect flux in the system. The value of flux can be obtained by measuring the reflection, with positive reflection indicating a value of flux close to half integer. While we studied Andreev reflections of relatively small density waves, given its wave origin and persistence in the GPE regime [39], we expect larger density waves to show similar behavior [69]. The density wave in lattice systems can be read out via the *in situ* atom density with state-of-the-art atom microscopes [70]. For the low-energy transport, the transport is carried by collective density wave excitations of the atomic condensate. In contrast to the nonequilibrium regime, the flux controls only the magnitude, but not the direction of the current into the leads. For a 1D Bose-liquid ring coupled to two leads, the low-energy current is known to be independent of flux [71]. Here, only the persistent current within the ring couples to the flux, while the transmission is flux independent. For low-energy currents, we believe this is also true for three lead systems, yielding the observed nondirectional currents. However, finite-size effects can change the effective coupling strength between ring and leads [71]. Flux causes substantial shifts of the energy levels in small rings, likely leading to a decreased effective ring-lead coupling and transmission for half flux.

Far from the ground state, the system is characterized by a substantially different dynamics. We analyze the dynamics for continuous noninteracting (Landauer formalism), dilute (continuous 2D GPE), and discrete strongly interacting limit (Bose-Hubbard lattice with Lindblad). The flux controls the direction of the current in all three regimes. Our work shows that control over the directionality is robust, appearing for zero, weak, and strong interactions, as well as for exactly one-dimensional and finite two-dimensional systems. By choosing the flux around $\Omega = (2k + 1)/4$, k being integer, we find a nonreciprocal behavior where we can direct the flow into either of the drains. With this effect we can switch the matter-wave between different output terminals to realize a transistor or a rotation sensor.

By sweeping the flux in time, the matter-wave experiences a time-dependent Aharonov-Bohm effect. This could be experimentally achieved by a constant acceleration of the
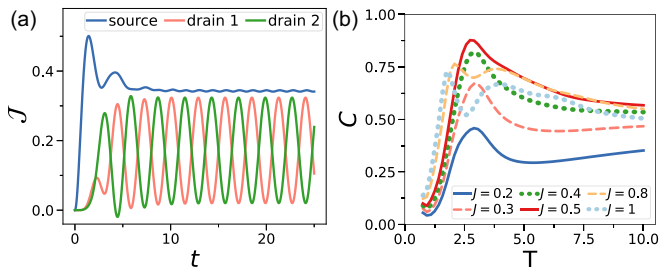
FIG. 5. Time-dependent flux $\Omega(t)$ for $L = 3$ ring sites. (a) Current $\mathcal{J}(t)$ in time t for a linearly increasing flux $\Omega(t) = t/T$ with driving period $T = 2.8$ and $J = \frac{1}{2}$. (b) dc/ac conversion efficiency $C = \Delta \mathcal{J}_{\text{drain}}/\langle \mathcal{J}_{\text{source}} \rangle$ measured as the drain current amplitude relative to the average source current against driving period T of the flux $\Omega(t) = t/T$. We have hard-core bosons with $L = 3$, $K = 1$, and $B_\alpha = 1$.

rotation affecting the ring or ramping the flux periodically up and down. This driving generates a sinusoidal modulation of the current in time. As a result, a constant source current is converted into an ac modulated current in the drains. We control the frequency and amplitude of the modulation via the change of the flux, with maximal conversion efficiency $C \approx 0.88$. In a reverse operation, this remarkable feature can be used as a sensor for time-dependent rotations $\Omega(t)$ by measuring the frequency of the current.

The time-dependent flux also allows us to study the time-dependent Aharonov-Bohm effect with cold atoms in a controlled environment, which has remained an open problem in other systems [51–54]. Depending on the cold-atom implementation, additional terms can appear in the effective Hamiltonian for the time-dependent driving of the flux, which have to be carefully studied in future work.

We provide the cold atom system that integrates switch-like and frequency generating capabilities. Our work relies on current experimental capabilities of the field, where we experimentally demonstrate the feasibility of the parameters of our simulations. Note that our setup is a special case of a much larger class of possible atomtronic setups. Inspired by vast applications of classical ring wave guides for electromagnetic fields [72–74], analogous atomtronic devices for directional couplers, frequency filters, or wave splitters could be designed. We hope to draw attention to this rich field for application in cold atom technologies, which to our knowledge has been barely explored.

[1] I. Bloch, J. Dalibard, and S. Nascimbene, Quantum simulations with ultracold quantum gases, Nat. Phys. **8**, 267 (2012).

[2] M. Keil, O. Amit, S. Zhou, D. Groswasser, Y. Japha, and R. Folman, Fifteen years of cold matter on the atom chip: promise, realizations, and prospects, J. Mod. Opt. **63**, 1840 (2016).

[3] L. Amico, D. Anderson, M. Boshier, J.-P. Brantut, L.-C. Kwek, A. Minguzzi, and W. von Klitzing, Colloquium: Atomtronic circuits: From many-body physics to quantum technologies, Rev. Mod. Phys. **94**, 041001 (2022).

[4] L. Amico, M. Boshier, G. Birkl, A. Minguzzi, C. Miniatura, L.-C. Kwek, D. Aghamalyan, V. Ahufinger, D. Anderson, N. Andrei *et al.*, Roadmap on atomtronics: State of the art and perspective, AVS Quantum Sci. **3**, 039201 (2021).

[5] L. Amico, G. Birkl, M. Boshier, and L.-C. Kwek, Focus on atomtronics-enabled quantum technologies, New J. Phys. **19**, 020201 (2017).

[6] D. McGloin, G. C. Spalding, H. Melville, W. Sibbett, and K. Dholakia, Applications of spatial light modulators in atom optics, Opt. Express **11**, 158 (2003).

[7] C. Ryu and M. G. Boshier, Integrated coherent matter wave circuits, New J. Phys. **17**, 092002 (2015).

[8] G. Gauthier, I. Lenton, N. M. Parry, M. Baker, M. Davis, H. Rubinsztein-Dunlop, and T. Neely, Direct imaging of a digital-micromirror device for configurable microscopic optical potentials, Optica **3**, 1136 (2016).

[9] D. Barredo, V. Lienhard, S. De Leseleuc, T. Lahaye, and A. Browaeys, Synthetic three-dimensional atomic structures assembled atom by atom, Nature (London) **561**, 79 (2018).

[10] B. T. Seaman, M. Krämer, D. Z. Anderson, and M. J. Holland, Atomtronics: Ultracold-atom analogs of electronic devices, Phys. Rev. A **75**, 023615 (2007).

[11] R. A. Pepino, J. Cooper, D. Z. Anderson, and M. J. Holland, Atomtronic Circuits of Diodes and Transistors, Phys. Rev. Lett. **103**, 140405 (2009).

[12] R. A. Pepino, Advances in atomtronics, Entropy **23**, 534 (2021).

[13] D. Z. Anderson, Matter waves, single-mode excitations of the matter-wave field, and the atomtronic transistor oscillator, Phys. Rev. A **104**, 033311 (2021).

[14] S. C. Caliga, C. J. Straatsma, A. A. Zozulya, and D. Z. Anderson, Principles of an atomtronic transistor, New J. Phys. **18**, 015012 (2016).

[15] S. C. Caliga, C. J. Straatsma, and D. Z. Anderson, Transport dynamics of ultracold atoms in a triple-well transistor-like potential, New J. Phys. **18**, 025010 (2016).

[16] S. C. Caliga, C. J. Straatsma, and D. Z. Anderson, Experimental demonstration of an atomtronic battery, New J. Phys. **19**, 013036 (2017).

[17] K. W. Wilsmann, L. H. Ymai, A. P. Tonel, J. Links, and A. Foerster, Control of tunneling in an atomtronic switching device, Commun. Phys. **1**, 91 (2018).

[18] C. Ryu, E. Samson, and M. G. Boshier, Quantum interference of currents in an atomtronic squid, Nat. Commun. **11**, 3338 (2020).

[19] S. Eckel, J. G. Lee, F. Jendrzejewski, N. Murray, C. W. Clark, C. J. Lobb, W. D. Phillips, M. Edwards, and G. K. Campbell, Hysteresis in a quantized superfluid 'atomtronic' circuit, Nature (London) **506**, 200 (2014).

[20] K. C. Wright, R. B. Blakestad, C. J. Lobb, W. D. Phillips, and G. K. Campbell, Driving Phase Slips in a Superfluid Atom Circuit with a Rotating Weak Link, Phys. Rev. Lett. **110**, 025302 (2013).

[21] A. Pérez-Obiol, J. Polo, and L. Amico, Coherent phase slips in coupled matter-wave circuits, Phys. Rev. Res. **4**, L022038 (2022).

[22] H. Kiehn, V. P. Singh, and L. Mathey, Implementation of an atomtronic squid in a strongly confined toroidal condensate, Phys. Rev. Res. **4**, 033024 (2022).

[23] C.-C. Chien, S. Peotta, and M. Di Ventra, Quantum transport in ultracold atoms, Nat. Phys. **11**, 998 (2015).

[24] A. J. Heeger, S. Kivelson, J. Schrieffer, and W.-P. Su, Solitons in conducting polymers, Rev. Mod. Phys. **60**, 781 (1988).

[25] M. Atala, M. Aidelsburger, J. T. Barreiro, D. Abanin, T. Kitagawa, E. Demler, and I. Bloch, Direct measurement of the zak phase in topological bloch bands, Nat. Phys. **9**, 795 (2013).

[26] H. Miyake, G. A. Siviloglou, C. J. Kennedy, W. C. Burton, and W. Ketterle, Realizing the Harper Hamiltonian with Laser-Assisted Tunneling in Optical Lattices, Phys. Rev. Lett. **111**, 185302 (2013).

[27] M. Aidelsburger, M. Atala, M. Lohse, J. T. Barreiro, B. Paredes, and I. Bloch, Realization of the Hofstadter Hamiltonian with Ultracold Atoms in Optical Lattices, Phys. Rev. Lett. **111**, 185301 (2013).

[28] G. Jotzu, M. Messer, R. Desbuquois, M. Lebrat, T. Uehlinger, D. Greif, and T. Esslinger, Experimental realization of the topological haldane model with ultracold fermions, Nature (London) **515**, 237 (2014).

[29] J.-P. Brantut, J. Meineke, D. Stadler, S. Krinner, and T. Esslinger, Conduction of ultracold fermions through a mesoscopic channel, Science **337**, 1069 (2012).

[30] S. Krinner, D. Stadler, D. Husmann, J.-P. Brantut, and T. Esslinger, Observation of quantized conductance in neutral matter, Nature (London) **517**, 64 (2015).

[31] D. Husmann, S. Uchino, S. Krinner, M. Lebrat, T. Giamarchi, T. Esslinger, and J.-P. Brantut, Connecting strongly correlated superfluids by a quantum point contact, Science **350**, 1498 (2015).

[32] M. Lebrat, P. Grišins, D. Husmann, S. Häusler, L. Corman, T. Giamarchi, J.-P. Brantut, and T. Esslinger, Band and Correlated Insulators of Cold Fermions in a Mesoscopic Lattice, Phys. Rev. X **8**, 011053 (2018).

[33] G. Gauthier, S. S. Szigeti, M. T. Reeves, M. Baker, T. A. Bell, H. Rubinsztein-Dunlop, M. J. Davis, and T. W. Neely, Quantitative Acoustic Models for Superfluid Circuits, Phys. Rev. Lett. **123**, 260402 (2019).

[34] S. Pandey, H. Mas, G. Drougakis, P. Thekkeppatt, V. Bolpasi, G. Vasilakis, K. Poulios, and W. von Klitzing, Hypersonic bose–einstein condensates in accelerator rings, Nature (London) **570**, 205 (2019).

[35] T. Haug, L. Amico, R. Dumke, and L.-C. Kwek, Mesoscopic vortex–meissner currents in ring ladders, Quantum Sci. Technol. **3**, 035006 (2018).

[36] T. Haug, R. Dumke, L.-C. Kwek, and L. Amico, Topological pumping in aharonov–bohm rings, Commun. Phys. **2**, 127 (2019).

[37] T. Haug, H. Heimonen, R. Dumke, L.-C. Kwek, and L. Amico, Aharonov-Bohm effect in mesoscopic Bose-Einstein condensates, Phys. Rev. A **100**, 041601(R) (2019).

[38] S. Safaei, L.-C. Kwek, R. Dumke, and L. Amico, Monitoring currents in cold-atom circuis, Phys. Rev. A **100**, 013621 (2019).

[39] T. Haug, R. Dumke, L.-C. Kwek, and L. Amico, Andreev-reflection and aharonov–bohm dynamics in atomtronic circuits, Quantum Sci. Technol. **4**, 045001 (2019).

[40] T. F. Haug, Quantum transport with cold atoms, Ph.D. thesis, National University of Singapore (Singapore), 2021.

[41] A. Ramanathan, K. C. Wright, S. R. Muniz, M. Zelan, W. T. Hill III, C. J. Lobb, K. Helmerson, W. D. Phillips, and G. K. Campbell, Superflow in a Toroidal Bose-Einstein Condensate: An Atom Circuit with a Tunable Weak Link, Phys. Rev. Lett. **106**, 130401 (2011).

[42] C. Ryu, P. W. Blackburn, A. A. Blinova, and M. G. Boshier, Experimental Realization of Josephson Junctions for an Atom SQUID, Phys. Rev. Lett. **111**, 205301 (2013).

[43] B. Eller, O. Oladehin, D. Fogarty, C. Heller, C. W. Clark, and M. Edwards, Producing flow in racetrack atom circuits by stirring, Phys. Rev. A **102**, 063324 (2020).

[44] D. Aghamalyan, M. Cominotti, M. Rizzi, D. Rossini, F. Hekking, A. Minguzzi, L.-C. Kwek, and L. Amico, Coherent superposition of current flows in an atomtronic quantum interference device, New J. Phys. **17**, 045023 (2015).

[45] T. Haug, J. Tan, M. Theng, R. Dumke, L.-C. Kwek, and L. Amico, Readout of the atomtronic quantum interference device, Phys. Rev. A **97**, 013633 (2018).

[46] Y. Aharonov and D. Bohm, Significance of electromagnetic potentials in the quantum theory, Phys. Rev. **115**, 485 (1959).

[47] Y. Gefen, Y. Imry, and M. Y. Azbel, Quantum Oscillations and the Aharonov-Bohm Effect for Parallel Resistors, Phys. Rev. Lett. **52**, 129 (1984).

[48] M. Büttiker, Y. Imry, and M. Y. Azbel, Quantum oscillations in one-dimensional normal-metal rings, Phys. Rev. A **30**, 1982 (1984).

[49] R. A. Webb, S. Washburn, C. P. Umbach, and R. B. Laibowitz, Observation of $\frac{h}{e}$ Aharonov-Bohm Oscillations in Normal-Metal Rings, Phys. Rev. Lett. **54**, 2696 (1985).

[50] Y. Imry, *Introduction to Mesoscopic Physics* (Oxford University Press on Demand, 2002), Vol. 2.

[51] D. Singleton and E. C. Vagenas, The covariant, time-dependent aharonov–bohm effect, Phys. Lett. B **723**, 241 (2013).

[52] J. Macdougall, D. Singleton, and E. C. Vagenas, Revisiting the marton, simpson, and suddeth experimental confirmation of the aharonov–bohm effect, Phys. Lett. A **379**, 1689 (2015).

[53] J. Jing, Y.-F. Zhang, K. Wang, Z.-W. Long, and S.-H Dong, On the time-dependent aharonov–bohm effect, Phys. Lett. B **774**, 87 (2017).

[54] S. R. Choudhury and S. Mahajan, Direct calculation of time varying aharonov-bohm effect, Phys. Lett. A **383**, 2467 (2019).

[55] D. Jaksch and P. Zoller, Creation of effective magnetic fields in optical lattices: the hofstadter butterfly for cold neutral atoms, New J. Phys. **5**, 56 (2003).

[56] Y.-J. Lin, R. L. Compton, K. Jiménez-García, J. V. Porto, and I. B. Spielman, Synthetic magnetic fields for ultracold neutral atoms, Nature (London) **462**, 628 (2009).

[57] J. Dalibard, F. Gerbier, G. Juzeliūnas, and P. Öhberg, Colloquium: Artificial gauge potentials for neutral atoms, Rev. Mod. Phys. **83**, 1523 (2011).

[58] T. Haug, R. Dumke, L.-C. Kwek, C. Miniatura, and L. Amico, Machine-learning engineering of quantum currents, Phys. Rev. Res. **3**, 013034 (2021).

[59] G. D. Pace, K. Xhani, A. M. Falconi, M. Fedrizzi, N. Grani, D. H. Rajkov, M. Inguscio, F. Scazza, W. J. Kwon, and G. Roati, Imprinting Persistent Currents in Tunable Fermionic Rings, Phys. Rev. X **12**, 041037 (2022).

[60] See Supplemental Material at http://link.aps.org/supplemental/10.1103/PhysRevA.107.L051303 for details on the Landauer formula, experiment and Gross-Pitaevskii equation.

[61] W. Bao, D. Jaksch, and P. A. Markowich, Numerical solution of the gross–pitaevskii equation for bose–einstein condensation, J. Comput. Phys. **187**, 318 (2003).

[62] P. Engels, I. Coddington, P. C. Haljan, V. Schweikhard, and E. A. Cornell, Observation of Long-Lived Vortex Aggregates in Rapidly Rotating Bose-Einstein Condensates, Phys. Rev. Lett. **90**, 170405 (2003).

[63] C. Weitenberg and J. Simonet, Tailoring quantum gases by floquet engineering, Nat. Phys. **17**, 1342 (2021).

[64] K. Wintersperger, C. Braun, F. N. Ünal, A. Eckardt, M. D. Liberto, N. Goldman, I. Bloch, and M. Aidelsburger, Realization of an anomalous floquet topological system with ultracold atoms, Nat. Phys. **16**, 1058 (2020).

[65] M. Fishman, S. R. White, and E. M. Stoudenmire, The ITen-sor Software Library for Tensor Network Calculations, SciPost Phys. Codebases **2022**, 4 (2022).

[66] P. Wittek and L. Calderaro, Extended computational kernels in a massively parallel implementation of the trotter–suzuki approximation, Comput. Phys. Commun. **197**, 339 (2015).

[67] H.-P. Breuer, F. Petruccione *et al.*, *The Theory of Open Quantum Systems* (Oxford University Press on Demand, 2002).

[68] C. Guo and D. Poletti, Dissipatively driven hardcore bosons steered by a gauge field, Phys. Rev. B **96**, 165409 (2017).

[69] A. J. Daley, P. Zoller, and B. Trauzettel, Andreev-Like Re-flections with Cold Atoms, Phys. Rev. Lett. **100**, 110404 (2008).

[70] J. F. Sherson, C. Weitenberg, M. Endres, M. Cheneau, I. Bloch, and S. Kuhr, Single-atom-resolved fluorescence imag-ing of an atomic mott insulator, Nature (London) **467**, 68 (2010).

[71] A. Tokuno, M. Oshikawa, and E. Demler, Dynamics of One-Dimensional Bose Liquids: Andreev-Like Reflection at *Y* Junctions and the Absence of the Aharonov-Bohm Effect, Phys. Rev. Lett. **100**, 140402 (2008).

[72] C. Y. Pon, Hybrid-ring directional coupler for arbitrary power divisions, IRE Trans. Microwave Theory Tech. **9**, 529 (1961).

[73] A. Yariv, Critical coupling and its control in optical waveguide-ring resonator systems, IEEE Photon. Technol. Lett. **14**, 483 (2002).

[74] P. Dong, N.-N. Feng, D. Feng, W. Qian, H. Liang, D. C. Lee, B. Luff, T. Banwell, A. Agarwal, P. Toliver *et al.*, Ghz-bandwidth optical filters based on high-order silicon ring resonators, Opt. Express **18**, 23784 (2010).